Radiation Dose Reduction in Digital Radiography Using Wavelet-Based Image Processing Methods

Haruyuki Watanabe*[a], Du-Yih Tsai*[a], Yongbum Lee [a], Eri Matsuyama [a], and Katsuyuki Kojima [b]

[a]Department of Radiological Technology, Graduate School of Health Sciences, Niigata University, 2-746, Asahimachi-dori, Chuo-ku, Niigata, 951-8518, Japan
[b]Department of Business Administration, Graduate School of Business Administration, Hamamatsu University, 1230, Miyakodacho, Kita-ku, Hamamatsu, 431-2102, Japan

ABSTRACT

In this paper, we investigate the effect of the use of wavelet transform for image processing on radiation dose reduction in computed radiography (CR), by measuring various physical characteristics of the wavelet-transformed images. Moreover, we propose a wavelet-based method for offering a possibility to reduce radiation dose while maintaining a clinically acceptable image quality. The proposed method integrates the advantages of a previously proposed technique, *i.e.,* sigmoid-type transfer curve for wavelet coefficient weighting adjustment technique, as well as a wavelet soft-thresholding technique. The former can improve contrast and spatial resolution of CR images, the latter is able to improve the performance of image noise. In the investigation of physical characteristics, modulation transfer function, noise power spectrum, and contrast-to-noise ratio of CR images processed by the proposed method and other different methods were measured and compared. Furthermore, visual evaluation was performed using Scheffe's pair comparison method. Experimental results showed that the proposed method could improve overall image quality as compared to other methods. Our visual evaluation showed that an approximately 40% reduction in exposure dose might be achieved in hip joint radiography by using the proposed method.

Keywords: Wavelet transform, image noise, radiation dose, image quality

1. INTRODUCTION

In the clinical implementation of digital radiography, it is imperative to use the appropriate level of radiation for the diagnostic task. It is known that a trade-off exists between noise level and radiation dose. On one hand, a high-dose radiation will lower the noise level but may give excess radiation doses to the patient. On the other hand, a low-dose radiation will lower the signal-to-noise ratio of the image and result in reducing the amount of image information. Thus, it is important to obtain radiological images that provide more diagnostic information at a lower radiation dose. So far, several investigators have reported that wavelet-based image processing techniques are effective in reduction of radiation dose [1-6]. The wavelet transforms can be used to divide an image into several frequency domains. The potential information in each image is retained, and extraction of the image information in each frequency domain is possible. Image noise can be reduced by performing wavelet de-noising technique in the frequency domain. However, to the best of our knowledge, little work has been done to investigate the relations of physical properties of wavelet-processed images and radiation dose reduction.

Furthermore, general image techniques based on the soft-threshold methods using wavelet transform will degrade the image resolution and consequently limit the visual performance. The most common cause of the decrease of resolution by using the conventional wavelet-based techniques is mainly due to the determination of reasonable wavelet coefficient threshold.

*harukiwa@d1.dion.ne.jp; tsai@clg.niigata-u.ac.jp; phone +81 25 227 0965; fax +81 25 227 0965

In this study, we propose a novel technique using wavelet-based image processing to reduce the noise while maintaining the resolution and contrast of the images. The reduction of the noise may result in the reduction of radiation dose. In order to validate the effect of employment of proposed technique on radiation dose reduction for digital radiography, images of the lumbar spine and hip joint phantoms, obtained from different dose levels in the standard range of X-ray energies, were quantitatively and qualitatively assessed.

2. WAVELET-BASED IMAGE PROCESSING

As shown in Figure 1, the proposed method for denoising radiographic images starts by decomposing the original image using the discrete wavelet transform, which results in different detail coefficients (horizontal, vertical, diagonal) of frequency. The images are then processed using sigmoid-type transfer curve for wavelet coefficient weighting adjustment (sigmoid), followed by soft-threshold operation.

Sigmoid-type transfer curve for wavelet coefficient weighting adjustment (sigmoid)

The sigmoid filter is used to enhance image contrast: the coefficients with great values and the coefficients of high resolution levels are heavily weighted [7]. In the wavelet decomposition of level *J*, the sigmoid-type transfer curves of wavelet coefficient can be expressed as follows:

$$w^{j}_{output}(m,n) = a \times \frac{1}{1+1/\exp\left[\dfrac{w^{j}_{input}(m,n)-c}{b}\right]} \times w^{j}_{input}(m,n) \quad [\%], \tag{1}$$

where $w^{j}_{input}(m, n)$ and $w^{j}_{output}(m, n)$ represent input and output values, respectively. In this study, the value of a was computed using equation (2):

$$a = 2 - \frac{(j-1)}{N}, \tag{2}$$

where N represents the maximum decomposition level. Consequently, if wavelet decomposition level j becomes smaller, the gradient of the graph obtained from equation (1) get greater. The constant c was determined using equation (3).

$$c = d + b \times \ln(a - 1.0), \tag{3}$$

where d is a constant used to determine inflection point of sigmoid curve, and b represents a constant to determine gradient of sigmoid curve. The values of d and b used in this study are 25 and 20, respectively [8].

Soft-threshold

The noise reduction technique of soft-threshold method which applies to additive noise is implemented using constant threshold of

$$\lambda = \sigma\sqrt{2\log_e(sample\_data)}, \tag{4}$$

where λ is the threshold value, σ is standard deviation of noise, and *sample_data* is the number of pixels of image [9]. The soft-threshold operator is defined by:

$$\dot{w}^j(m,n) = \begin{cases} w^j(m,n) + \lambda, & w^j(m,n) < -\lambda \\ 0, & -\lambda \le w^j(m,n) \le \lambda \\ w^j(m,n) - \lambda, & w^j(m,n) > \lambda \end{cases}, \quad (5)$$

where $w^j(m,n)$ is the wavelet coefficient at level j. The amplitude of most of the wavelet components is noise only. This method is to set to zero all components which are lower than a threshold related to noise level and appropriately shrink the rest of the components by an amount equal to the threshold.

Finally, the modified wavelet coefficients using the sigmoid and the soft-threshold are transformed back into its original domain by use of the inverse wavelet transform to obtain an optimal image.

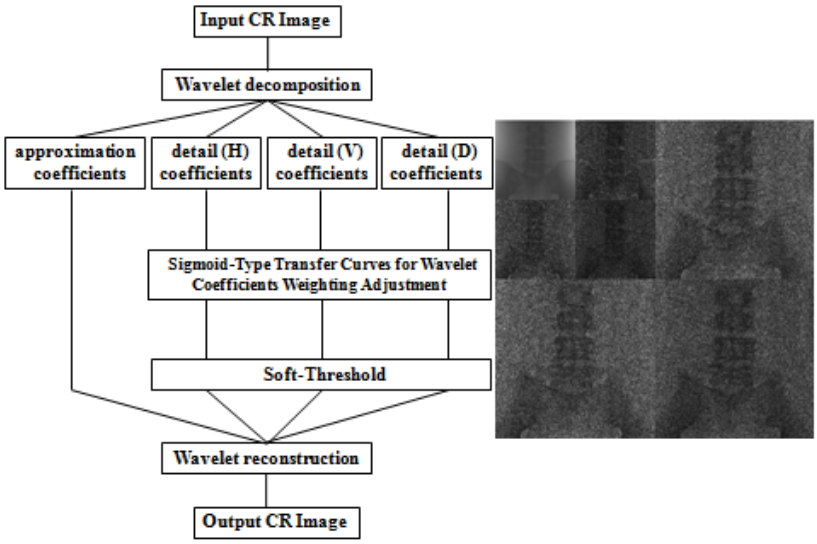

Fig. 1 Flow chart of the proposed method.

3. METHODS AND MATERIALS

3.1 Experiments setup

A CR imaging system (FCR XG-1, Fuji Photo Film, Tokyo, Japan) was used in the study. An imaging plate (ST-V_N) was used as a detector. The pixel size and the quantization level of the images used were 0.1 mm and 10 bits. Radiographs were taken with radiation quality of RQA-5 (HVL=7.1 mm Al, 21 mm Al additional filtration). The image data used in this study consisted of 20 phantom images. The phantom images were evaluated with respect to various physical properties.

3.2 Physical properties measurement

In order to validate the usefulness of the proposed method (sigmoid+threshold), this filter was compared to other filters using wavelet-based image processing. In the conventional methods using soft-threshold, wavelet basis functions of Haar (Lv4), Daubechies4 (Lv4), and Coiflets4 (Lv4) were adopted for image processing. In addition, a sigmoid-type transfer curve for wavelet coefficient weighting adjustment (sigmoid) together with the use of Daubechies4 (Lv4) was also independently adopted. The proposed method and the above-described four filters were applied to the original images for performance evaluation.

3.2.1 Modulation Transfer Function (MTF)

Evaluation of spatial resolution property was performed by measuring the MTFs. The MTFs were measured with an angled-edge method. A tungsten plate (1 mm thickness) was used as an edge device. The direction of the edge was oriented with a small angle (2°–3°). The edge is made of a 100-μm-thick sharp edged tungsten plate and its dimension was 10×10 cm^2. Images of the edge were acquired with an exposure of 4.63×10^{-7} C/kg (50 mAs). After the image of the edge was scanned, the digital image data were transferred to a computer. The edge spread function (ESF) in the direction perpendicular to the edge was then obtained. To reduce the noise in the edge profile, 20 representations of sampled ESF were generated from the region of interest (ROI). The ESFs were then differentiated to obtain the line spread functions and the presampled MTFs were similarly deduced by Fourier transformation. The details of the processing method are given elsewhere [10, 11].

3.2.2 Noise Power Spectrum (NPS)

The NPS measurements were made by exposing the imaging plates to a uniform beam of radiation. For determination of the NPS, the entrance exposure (air kerma) for the images was 4.63×10^{-7} C/kg. To remove long-range background trends, a two-dimensional 2nd order polynominal was fitted and subtracted. For the calculation, the central portion of each obtained uniform image was divided into 4 non-overlapping regions, 256×256 in size (80 in total). The NPS was calculated by applying the fast Fourier transform to each ROI and averaging the resulting spectrum estimates. The details of the methodology are reported elsewhere [12, 13].

3.2.3 Contrast-to-Noise Ratio (CNR)

The CNR measurements were made using an acrylic disk on the Burger's phantom. An ROI with a size of 30×30 pixels was selected at the center of disk and neighbour background. CNR can be calculated by use of the following equation:

$$CNR = \frac{m_{\mathbf{BG}} - m_{\mathbf{disk}}}{\sigma_{\mathbf{BG}}}\ , \tag{6}$$

where m_{BG}, $m_{disk,}$ and σ_{BG} represent the mean of the background, mean of the disk, and standard deviation of background, respectively.

3.2.4 Peak Signal-to-Noise Ratio (PSNR)

The PSNR was obtained from the area covering the entire field of the image using human body phantom. The PSNR is given by the squared root of the ratio of the peak value of gray level squared to the mean square error (MSE). The PSNR and MSE were obtained using the following equations:

$$PSNR = 20\log_{10}(PV_{\max} / \sqrt{MSE}) \qquad [\mathrm{dB}]\ , \tag{7}$$

$$MSE\ =\ \frac{1}{M \times M'}\sum_{i=1}^{M}\sum_{j=1}^{M'}(orig\ \_\ pixel_{i,j} - comp\ \_\ pixel_{i,j})^2\ , \tag{8}$$

where $PV_{\max}$ refers to maximum pixel value. The M and M′ are matrix sizes of the original and processed images, respectively.

3.2.5 Visual Evaluation

In order to evaluate the relationship between radiation dose and image quality, four X-ray images, *i.e.,* an anterior-posterior (AP) and an oblique (Lauenstein) projections of the hip-joint, as well as an AP and the lateral views of the lumbar were obtained by using a human body phantom. These four images were taken with four different radiation levels,

i.e., 50/100, 64/100, 80/100, and 100/100, as compared to the reference level that is commonly used in clinical radiology practice. The images obtained with the human body phantom and those used for measuring basic physical properties were processed using wavelet transforms.

Visual evaluation was conducted by five experienced radiological technologists. The images were displayed on a liquid crystal display (1280×1024 matrix, LCD-1980SXi, Nippon Electric Company, Tokyo, Japan). Statistical significance was tested using Scheffe's method of paired comparisons. The method of paired comparisons calculates the score of each image by comparative assessment between all possible pairs of images. Comparisons were made by six possible combinations, that is, Haar (Lv4)-processed image, Daubechies4 (Lv4)-processed image, Coiflets4 (Lv4)-processed image, sigmoid filter-processed image, sigmoid+threshold filter-prosessed and the original image. Conditions for the visual evaluation, including window level, window width, and display image size were fixed. Each observer independently reviewed the images. The reading time was not limited.

4. RESULTS

4.1 MTF

Figure 2 shows the MTFs for the original image and five images processed by various wavelet transforms. The MTF of sigmoid is superior to the original image at the entire spatial frequency range, followed by that of sigmoid+threshold which is slightly lower to sigmoid filter. In contrast, the MTFs obtained from the three wavelet-based filters of soft-threshold methods are slightly lower than the original one. Of the three filters, Haar basis function shows the highest MTF, followed by Daubechies and Coiflets.

4.2 NPS

Figure 3 shows the NPS values. The NPS values of the sigmoid have pronounced increase as compared with that of the original image. In contrast, the NPS values of sigmoid+threshold and three soft-threshold methods have noticeable decrease. It is noted that the NPS profile of Haar function fluctuates. As illustrated in Fig. 3, the NPS values for sigmoid-processed images show the highest rank, followed by original, sigmoid+threshold, Haar, Daubechies, and Coiflets.

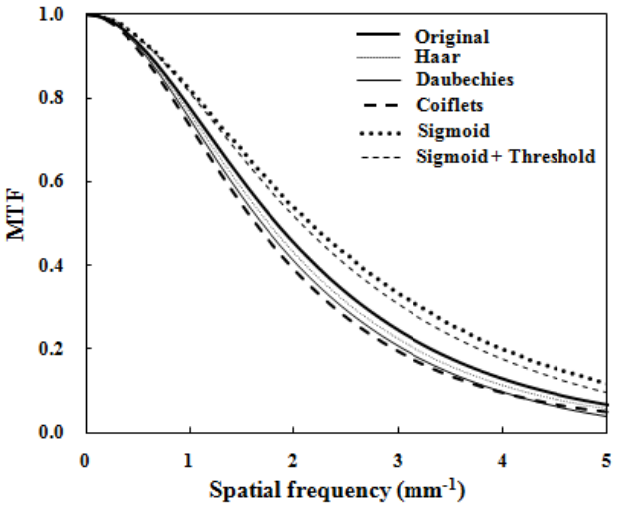

Fig. 2 MTFs of the original, Haar, Daubechies, Coiflets, Sigmoid, and Sigmoid+Threshold filter-processed images in the horizontal direction.

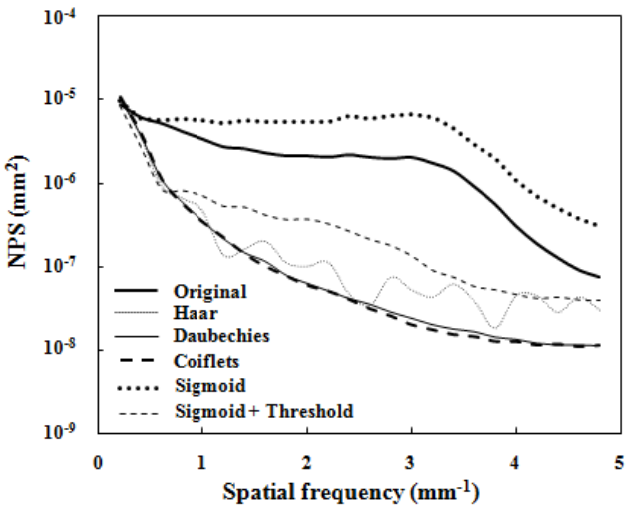

Fig. 3 NPSs of the original, Haar, Daubechies, Coiflets, Sigmoid, and Sigmoid+Threshold filter-processed images in the horizontal direction.

4.3 CNR

Figure 4(a) illustrates the CNRs obtained with acrylic disk images. Figure 4(b) and (c) depicts an example of the processed images including the original one and the corresponding disk profiles obtained from the central portion of the images. The CNR values of three soft-threshold methods are superior to the original image. However, the CNR value of sigmoid shows slightly lower compared to that of the original image. The CNR value of sigmoid+threshold is approximately intermediate between the original image and soft-threshold methods. As shown in Fig. 4(b), the sigmoid-processed image has higher spatial resolution compare to original image in shape, although it has the smallest CNR values. Haar image generated blocking artifacts. Furthermore, Daubechies and Coiflets images show considerable amount of blur. In addition, as shown in Fig. 4(c), the contrast of sigmoid image increases as compared to that of any other image.

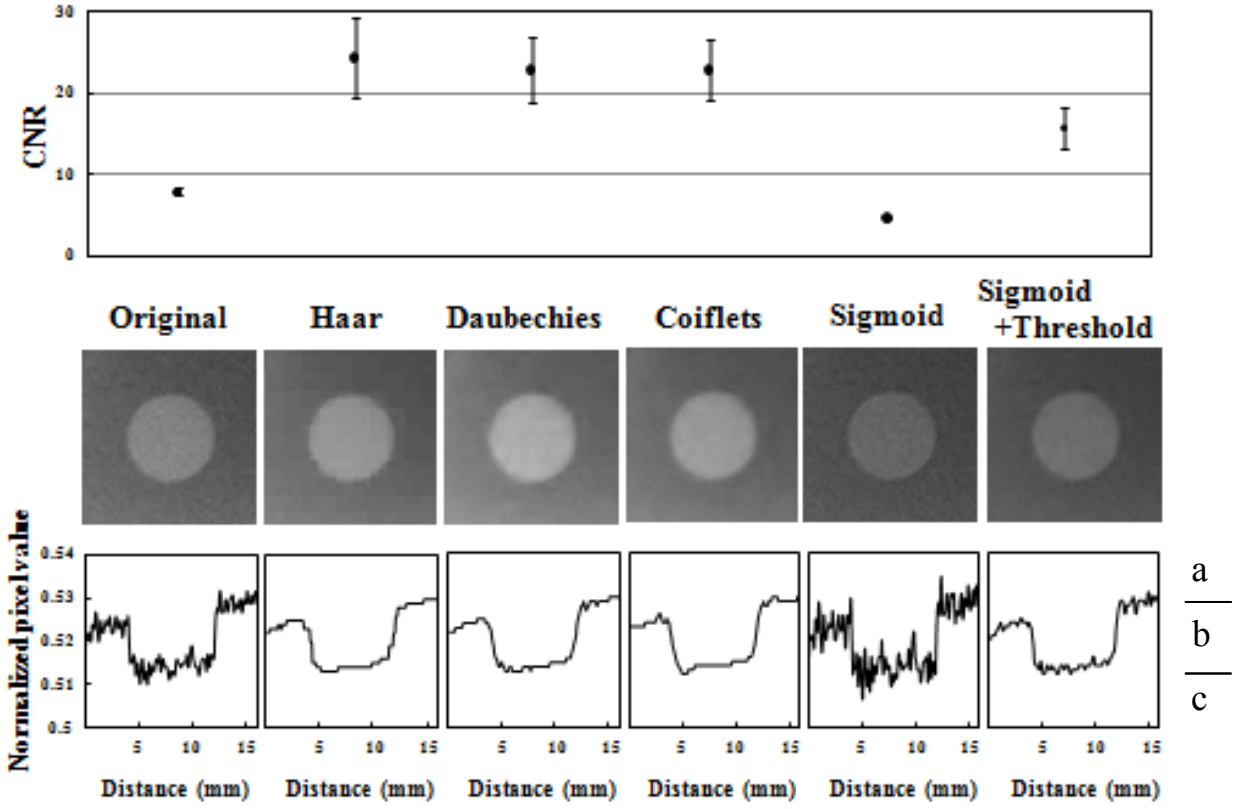

Fig. 4 (a) CNRs value of the original image, together with that of Haar, Daubechies, Coiflets, Sigmoid, and Sigmoid+Threshold filter processed images. (b) Acrylic disk images of the original and the five image processed images. (c) The corresponding disk profiles of the images shown in (b).

4.4 PSNR

Figure 5 shows the relationship between the radiation dose ratio and the PSNRs. The PSNRs in Fig. 5(a), (b), (c) and (d) were obtained from hip joint (AP), hip joint (Lauenstein), lumbar (AP) and lumbar (lateral), respectively. Note that the PSNRs of three soft-threshold methods have not much changed. They show the similar results, even if the portions examined are different. The PSNR of the sigmoid-processed image shows noticeable decrease as compared to that of the three soft-threshold methods. The PSNR of the sigmoid+threshold is slightly higher compare to that of the sigmoid. The PSNRs of sigmoid and sigmoid+threshold tend to decrease slightly with the reduction of exposure dose. However, the PSNRs of the soft-threshold methods show insignificant change.

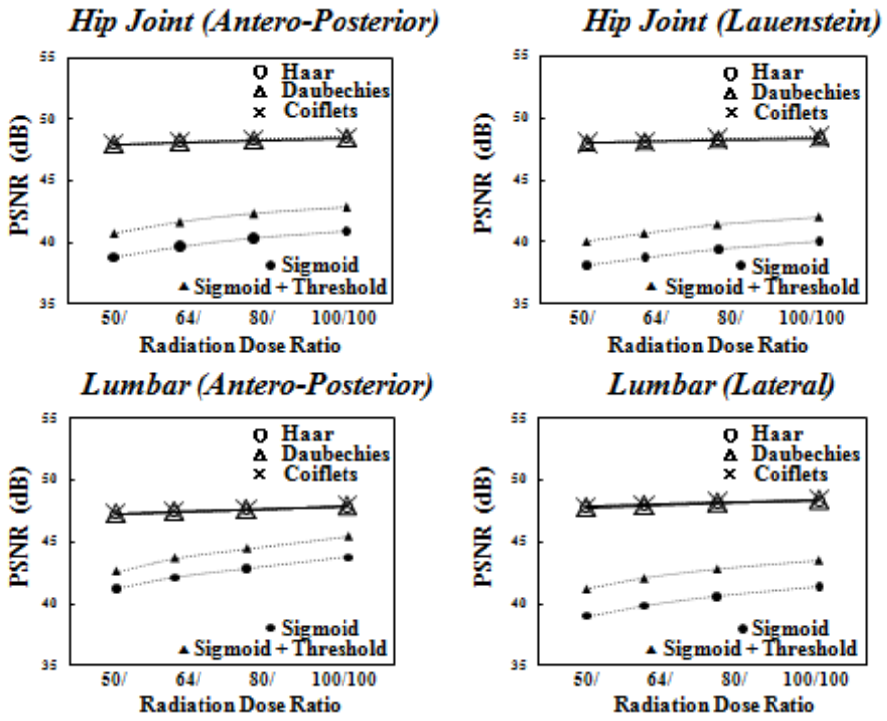

Fig. 5 PSNRs of Haar, Daubechies, Coiflets, Sigmoid, and Sigmoid+Threshold filters in Hip Joint (Antero-Posterior), Hip Joint (Lauenstein), Lumbar (Antero-Posterior), and Lumbar (Lateral).

4.5 Visual Evaluation

Figure 6 illustrates visual evaluation results for hip joint (AP) and the lumbar (AP) view using Scheffe's method of paired comparisons. Although, the results for hip joint (Lauenstein) and the lumbar (lateral) were not shown, the results of visual evaluation shows the same trend. In the case of hip joint radiographs, sigmoid and sigmoid+threshold provide excellent results compared to other images up to 80/100 radiation dose ratio. When radiation dose ratio is 64/100, sigmoid+threshold is superior to other images. However, sigmoid and sigmoid+threshold show unsatisfactory result when radiation dose rate is 50/100. In the case of lumbar radiographs, sigmoid+threshold results in the same compare to the original image up to 80/100 radiation dose rate. As a whole, sigmoid does not provide satisfactory results compare to other images. In other words, sigmoid filter is not effective for lumbar radiographs.

The soft-threshold methods do not exceed the original image in all cases. Among different wavelet basis of soft-threshold methods, Haar basis function results in a significant lower rating compared to other basis functions (Daubechies and Coiflets) at 80/100 radiation dose ratio in lumbar radiography.

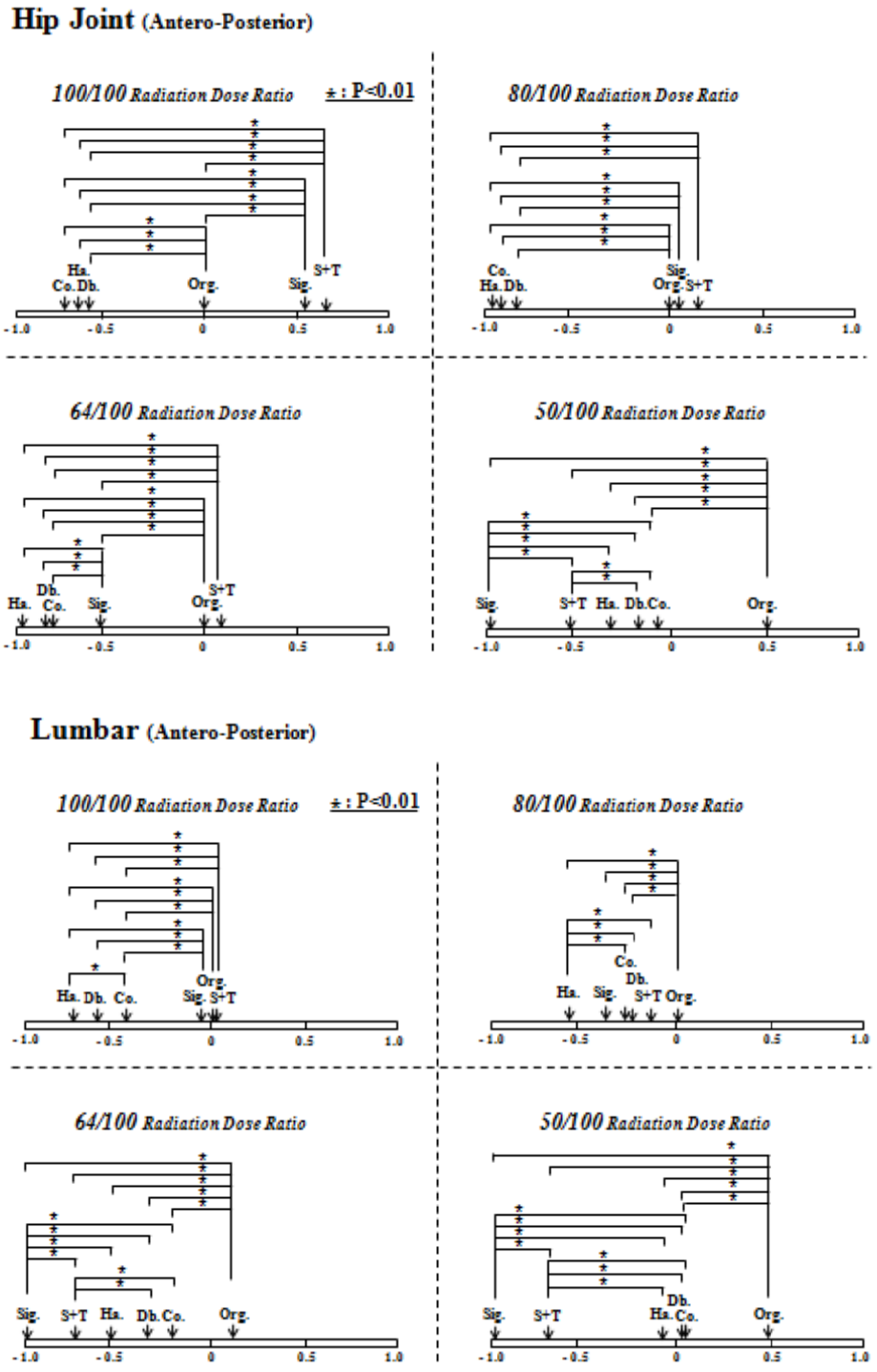

Fig. 6 Visual evaluation of Haar, Daubechies, Coiflets, Sigmoid, and Sigmoid+Threshold filters in Hip Joint (Antero-Posterior) and Lumbar (Antero-Posterior) at each radiation dose ratio.

5. DISCUSSION

We observed that the images processed by using the five adopted wavelet filters have considerable differences in physical properties. Especially, the physical properties of the images processed by using sigmoid function and soft-threshold methods show distinguished differences. The proposed method and sigmoid filter improve both spatial resolution property (Fig. 2) and image contrast (Fig. 4(a) and (b)). The sigmoid filter was designed to enhance image contrast. The effects of the use of sigmoid filter on contrast enhancement were shown in Fig. 4(c). Nevertheless, in the NPS measurement (Fig. 3), noise characteristics were improved by using soft-threshold methods. However, in contrast, effect of deteriorated blur appears on acrylic disk images. These results suggest that soft-threshold methods were not adequate for clinical application in its current form.

The proposed method incorporated with sigmoid and soft-threshold algorisms. As a result, the proposed method shows better spatial resolution and better noise properties as shown in Fig. 2 and 3. This method results in moderate CNR and PSNR values compared to other filters as shown in Fig. 4 and Fig. 5, respectively. Furthermore, a visual evaluation was performed in addition to the investigation of physical characteristics. Our evaluation results show that the use of proposed method can visually improve image quality and is comparable to the original image up to 64/100 radiation dose ratio in hip joint radiography. The usefulness of proposed method was demonstrated quantitatively and qualitatively by its application to a reduction of approximately 40% in exposure dose.

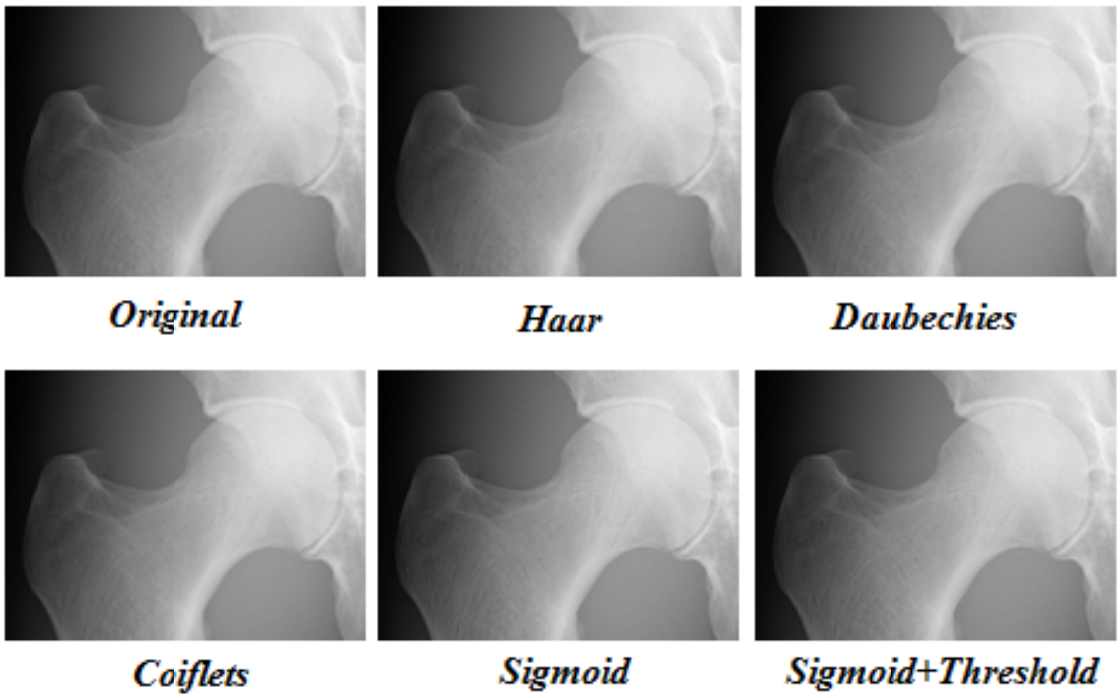

Fig. 7 Phantom images without and with image processing in hip joint (Lauenstein).

6. CONCLUSION

In this study, we investigated the effect of the use of wavelet transform on dose reduction in CR. The physical properties of the processed CR images were measured and compared. In the investigation of physical properties, the experimental results confirmed that the soft-threshold method can significantly reduce noise level and sigmoid method can effectively improve resolution characteristic. The proposed method provides not only better spatial resolution but also superior noise characteristics. Our visual evaluation showed that an approximately 40% reduction in exposure dose might be achieved with the proposed method in hip joint radiography.

REFERENCES

[1] M. Jansen, G. Uytterhoeven and A. Bultheel, "Image De-noising by Integer Wavelet Transforms and Generalized Cross Validation," Med. Phys. 26(4), 622-630 (1999).
[2] M. D. Harpan, "A Computer Simulation of Wavelet Noise Reduction in Computed Tomography," Med. Phys. 26(8), 1600-1606 (1999).
[3] T. Okamoto, S. Furui, H. Ichiji, S. Yoshino, J. Lu and T. Yanagi, "Noise Reduction in Digital Radiography Using Wavelet Packet Based on Noise Characteristics," J. Signal Processing 8(6), 485-494 (2004).
[4] O. Tischenko, C. Hoeschen and E. Buhr, "Reduction of Anatomical Noise in Medical X-Ray Images," Radiation Protection Dosimetry 114(1), 69-74 (2005).
[5] R. J. Ferrari and R. Winsor, "Digital Radiographic Image Denoising Via Wavelet-Based Hidden Markov Model Estimation," J. Digit. 18(2), 154-167 (2005).
[6] N. Yasuda, Y. Ishikawa and Y. Kodera, "Improvement of Image Quality in Chest MDCT Using Nonlinear Wavelet Shrinkage with Trimmed-thresholding," Jpn. J. Radiol. Technol. 61(12), 1599-1608 (2005).
[7] Y. Lee, D. Y. Tsai and T. Suzuki, "Contrast Enhancement of Medical Images Using Sigmoid-type Transfer Curves for Wavelet Coefficient Weighting Adjustment," Jpn. J. Medical Imaging and Information science 25(3), 48-53 (2008).
[8] D. Y. Tsai, Y. Lee and S. Sakaguchi, "A Preliminary Study of Wavelet-Coefficient Transfer Curves for the Edge Enhancement of Medical Images," Jpn. J. Medical and Biological Engineering 40(2), 20-24 (2002).
[9] D. L. Donoho, "De-noising by Soft-thresholding," IEEE Trans. 41(3), 613-627 (1995).
[10] E. Samei, J. Flynn and D. A. Reimann, "A Method for Measuring the Presampled MTF of Digital Radiographic Systems Using an Edge Test Device," Med. Phys. 25(1), 102-113 (1998).
[11] M. Flynn and E. Samei, "Experimental Comparison of Noise and Resolution for 2k and 4k Storage Phosphor Radiography Systems," Med. Phys. 26(8), 1612-1623 (1999).
[12] U. Neitzel, S. Gunther-Kohfahl, G. Borasi and E. Samei, "Determination of Detective Quantum Efficiency of a Digital X-Ray Detector: Comparison of Three Evaluations Using a Common Image Data Set," Med. Phys. 31(8), 2205-2211 (2004).
[13] E. Samei and M. J. Flynn, "An Experimental Comparison of Detector Performance for Computed Radiography Systems," Med. Phys. 29(4), 447-459 (2002).